

Spin dynamics of the planar kagome lattice ferromagnet with four-site ring exchange processes

Jonas Becker and Stefan Wessel

*Institut für Theoretische Festkörperphysik, JARA-FIT and JARA-HPC,
RWTH Aachen University, 52056 Aachen, Germany*

(Dated: March 18, 2022)

By means of quantum Monte Carlo simulations, combined with a stochastic analytic continuation, we examine the spin dynamics of the spin-1/2 planar (XY) ferromagnet on the kagome lattice with additional four-site ring exchange terms. Such exchange processes were previously considered to lead into an extended Z_2 quantum spin liquid phase beyond a quantum critical point from the XY-ferromagnet. We examine the dynamical spin structure factor in the non-magnetic regime and probe for signatures of spin fractionalization. Furthermore, we contrast our findings and the corresponding energy scales of the excitation gaps in the ring exchange model to those emerging in a related Balents-Fisher-Girvin model with a Z_2 quantum spin liquid phase, and monitor the softening of the magnon mode upon approaching the quantum critical point from the XY-ferromagnetic regime.

Competing interactions are an essential ingredient for stabilizing non-magnetic ground states of quantum magnets that exhibit topological order^{1,2}. The exploration of such quantum spin liquid (QSL) states is thus at the forefront of current research in condensed matter physics³⁻⁵. For this purpose, it is particularly valuable that several model systems have been conceived, which were proven to stabilize gapped QSL states in extended parts of their ground state phase diagrams. Prominent examples in this respect are Kitaev's toric-code and the honeycomb-lattice model^{6,7}, as well as the kagome lattice-based Balents-Fisher-Girvin (BFG) model⁸. For the latter system, the presence of an extended Z_2 -QSL phase can be derived, e.g., from a perturbative consideration, in which the bare spin-1/2 model maps onto an effective easy-axis spin-model with ring exchange processes on the kagome lattice's bow-ties, within a constrained low-energy manifold of states with zero total longitudinal magnetization on each (six-site) hexagon of the kagome lattice. The BFG model was furthermore shown to harbor fractionalized spin excitations and topological order in the QSL regime based on a formal equivalence to a particular quantum dimer (QD) model⁸. Such QD models have an exactly solvable limit, the Rokhsar-Kivelson point, at which the ground state is an exact superposition of all valid dimer coverings⁹, akin to a short-ranged resonating valence bond (RVB) state^{10,11}. In the meantime, the characterization of the QSL phase in the BFG model and variants thereof has been extended in various aspects, including the topological degeneracy and the corresponding contribution to the ground state entanglement, as well as the fractionalization of magnetic excitations¹²⁻¹⁹. Some of this progress was possible because the BFG model can be examined by sign-problem free, unbiased quantum Monte Carlo (QMC) simulations.

More recently, Dang, Inglis and Melko considered a spin-1/2 model with a direct competition between bare bow-tie ring exchange processes – which emerged only perturbatively within the BFG model – and a ferromagnetic nearest neighbor transverse spin exchange²⁰. More specifically, this J - K model is described by the following

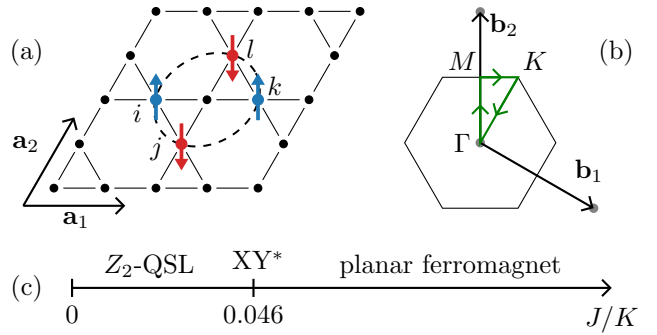


FIG. 1. (a) Kagome lattice with nearest neighbor (solid lines) and bow-tie ring exchange terms (dashed ellipse) of the J - K model. The latter processes are indicated for a bow-tie with edges i, j, k and l , along with a spin configuration that gets rotated by the exchange term $P_{i,j,k,l}$. (b) First Brillouin zone (BZ) along with the path $\Gamma \rightarrow M \rightarrow K \rightarrow \Gamma$ (green lines). (c) Ground state phase diagram of the J - K model from Ref. 20.

spin-1/2 Hamiltonian,

$$H = -J \sum_{\langle i,j \rangle} B_{i,j} - K \sum_{\langle i,j,k,l \rangle} P_{i,j,k,l}. \quad (1)$$

The summation of the transverse (XY) spin exchange, $B_{i,j} = S_i^+ S_j^- + S_i^- S_j^+$, extends over the nearest neighbor bonds on the kagome lattice, and the summation of the transverse ring exchange processes, $P_{i,j,k,l} = S_i^+ S_j^- S_k^+ S_l^- + S_i^- S_j^+ S_k^- S_l^+$, over all bow-ties on the kagome lattice, cf. Fig. 1(a) for an illustration. This model can be studied by sign-problem-free QMC simulations for positive values of J and K , using a multi-branch cluster update scheme^{21,22}. For $K = 0$, the ground state is a planar XY-ferromagnet, i.e., a superfluid in the equivalent hard-core boson representation. The ring exchange processes reduce the ferromagnetic alignment, and the authors of Ref. 20 identified a continuous quantum phase transition at a critical value of $K/J \approx 21.8$ ($J/K \approx 0.046$) to a large- K phase, which exhibits no

apparent symmetry breaking, cf. Fig. 1(c). By analogy to the BFG model, they concluded that (i) the large- K regime of the J - K model is a gapped Z_2 -QSL phase, and (ii) the quantum phase transition is a candidate for the XY^* universality class, in view of the fractionalization of the magnetic excitations within Z_2 -QSLs and the condensation of the spinons at the transition (a correspondingly large value of the anomalous exponent η was not determined in Ref. 20). Regarding the correspondence between the J - K and the BFG model, we note that (i) the ring exchange is an emerging low-energy process in the BFG model, while it is the leading term in the large- K regime of the J - K model, (ii) the J - K model does not feature an explicit constraint on the hexagonal magnetizations – within the QD model description, this allows for monomer defects to enter the low-energy manifold of the J - K model in addition to perfect dimer coverings. In view of these differences, it is thus worthwhile to examine the J - K model using probes that allow us to gain additional insight into the nature of its large- K regime. A powerful diagnostic approach to identify possible QSL phases are spectroscopic measurements probing, e.g., for scattering continua from fractionalized spin excitations.

Here, we thus examine in particular the spin dynamics of the J - K model in terms of the dynamical spin structure factor (DSSF), in order to probe for signatures of QSL physics in the large- K regime. We profit from recent QMC studies of the DSSF of the BFG model, which explicitly uncovered the fractionalized magnetic excitations in the established QSL regime^{18,19}. Below, we therefore address also the similarities and differences between these two models. In addition, we study the evolution of the DSSF upon varying the ratio J/K .

To calculate the DSSF of the J - K model, we performed QMC simulations using the sampling method from Ref. 19: We consider finite rhombic systems with $N_s = 3L^2$ lattice sites and periodic boundary conditions along both lattice directions $\mathbf{a}_1, \mathbf{a}_2$ in Fig. 1(a), with the unit cell distance fixed to $a = 1$. To formulate the DSSF on the three-sublattice kagome lattice, we denote by $\mathbf{S}_{i,\alpha}$ the spin at position $\mathbf{r}_{i,\alpha}$ on sublattice $\alpha = 1, 2, 3$ in the i -th unit cell ($i = 1, \dots, L^2$). We then obtain 3×3 correlation-matrices $S_{\alpha,\beta}^{+-}(\mathbf{k}, \omega) = \int dt e^{-i\omega t} \langle S_{\mathbf{k},\alpha}^+(t) S_{-\mathbf{k},\beta}^-(0) + S_{\mathbf{k},\alpha}^-(t) S_{-\mathbf{k},\beta}^+(0) \rangle$ for the transverse, and $S_{\alpha,\beta}^{zz}(\mathbf{k}, \omega) = \int dt e^{-i\omega t} \langle S_{\mathbf{k},\alpha}^z(t) S_{-\mathbf{k},\beta}^z(0) \rangle$ for the longitudinal channel respectively, where $\mathbf{S}_{\mathbf{k},\alpha} = (1/L) \sum_i e^{-i\mathbf{k} \cdot \mathbf{r}_{i,\alpha}} \mathbf{S}_{i,\alpha}$. We examine separately the traces over the correlation-matrices in each channel, $S^{+-}(\mathbf{k}, \omega) := \sum_{\alpha} S_{\alpha,\alpha}^{+-}(\mathbf{k}, \omega)$, and $S^{zz}(\mathbf{k}, \omega) := \sum_{\alpha} S_{\alpha,\alpha}^{zz}(\mathbf{k}, \omega)$, respectively, which contain the sum over the correlation-matrix eigenvalues of the spectral functions at each fixed momentum transfer \mathbf{k} from the first Brillouin zone (BZ). The BZ is shown in terms of the reciprocal lattice vectors $\mathbf{b}_1, \mathbf{b}_2$ in Fig. 1(b). In the following, we show QMC data for systems with $L = 12$. Simulations performed for $L = 18$ at selected parameter sets returned similar results. To target the ground state regime, the temperature T was adapted

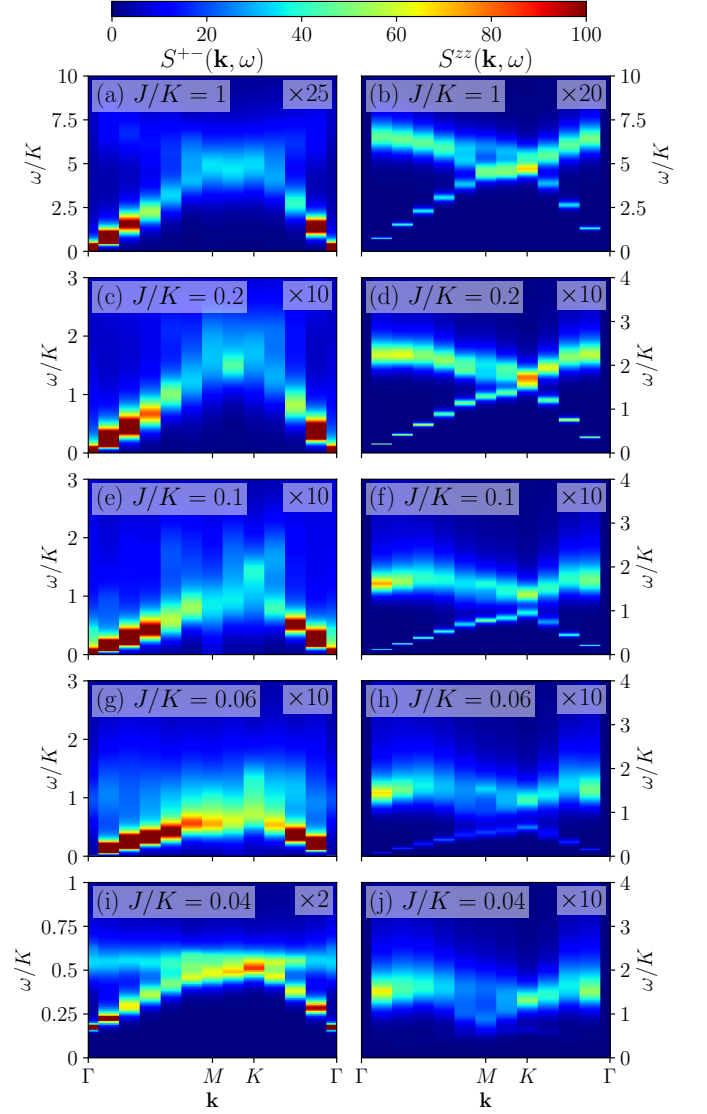


FIG. 2. DSSF $S^{+-}(\mathbf{k}, \omega)$ (left panels) and $S^{zz}(\mathbf{k}, \omega)$ (right panels) of the J - K model along the BZ path $\Gamma \rightarrow M \rightarrow K \rightarrow \Gamma$ [cf. Fig. 1(b)] for different ratios J/K from QMC simulations. To fit to a common scale, the intensities were multiplied by individual factors, which are provided in the upper right corner of each panel separately.

to $J/(2L)$ accordingly^{18,19}, and simulated annealing was used during the initial stage of the thermalization phase to improve equilibration. In order to extract the DSSF from the QMC simulations, we measured the transverse imaginary-time displaced spin-spin correlation functions and accessed the longitudinal correlations directly in Matsubara frequency space^{23,24}, using the stochastic analytic continuation method in the formulation of Ref. 25 to obtain the spectral functions in real frequencies for both cases. We performed the analytic continuations independently for the three correlation-matrix eigenvalues for each given momentum \mathbf{k} , in order to enhance the spectral resolution as detailed in Ref. 19.

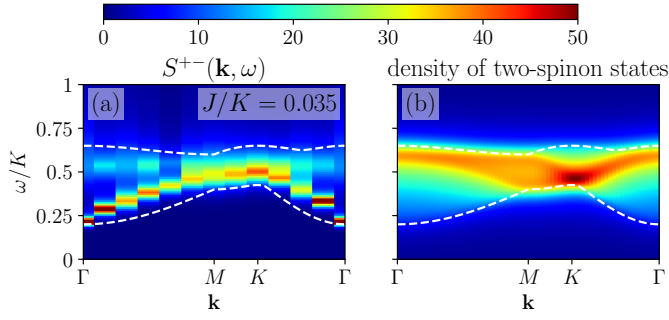


FIG. 3. (a) DSSF $S^{+-}(\mathbf{k}, \omega)$ of the J - K model for $J/K = 0.035$ along the BZ path $\Gamma \rightarrow M \rightarrow K \rightarrow \Gamma$. (b) Density of two-spinon states within the tight-binding model with $t = 0.025K$, and $\Delta_s = 0.25K$. In both panels, dashed lines indicate the lower and upper threshold of the two-spinon continuum within the tight-binding model.

We begin the investigation of the DSSF in the XY-ferromagnetic regime of the J - K model, cf. Fig. 1(c). The evolution of the DSSF upon varying J/K is shown in Fig. 2. For $J/K = 1$, (top panels) we observe the characteristic features of the XY-ferromagnetic regime (similar to the J -only limit ($K = 0$), cf. Ref. 19): In the transverse channel, $S^{+-}(\mathbf{k}, \omega)$, the spectral weight is dominantly contributed by a gapless low-energy magnon mode, i.e., the Goldstone soft-mode from the $U(1)$ symmetry breaking.

While the Goldstone mode contributes also some (weaker) spectral weight to $S^{zz}(\mathbf{k}, \omega)$, the longitudinal channel is dominated by optical magnons above $\omega \approx 5K$, with a dispersion maximum at the Γ -point. Upon reducing J/K , the overall energy scale of these excitations decreases correspondingly, cf. Fig. 2, along with a reduction of the spin wave velocity of the lower magnon mode (estimated from the slope of the Goldstone mode near the Γ -point). The bottom panels of Fig. 2, for $J/K = 0.04$, reside beyond the quantum phase transition, and exhibit finite excitation gaps in both channels, in accord with a gapped, non-ferromagnetic ground state.

The transverse channel for $J/K = 0.035$, which resides even further beyond the quantum critical point, is shown in Fig. 3(a). Apart from a slightly larger gap of about $\Delta_T \approx 0.24K$, it features a very similar overall structure as the DSSF for $J/K = 0.04$: The spectral weight is dominantly concentrated along the lower edge of the spectral support. This differs from the more broadly extended distribution of the spectral weight in the DSSF for the QSL regime of the BFG model^{18,19}: in the latter case, the transverse DSSF indeed compares well to a tight-binding model of two-spinon continuum states¹⁹, providing a smoking-gun signature for fractionalized spin excitations.

For a direct comparison to the J - K model data, the two-spinon DSSF is shown in Fig. 3(b). For the latter, the two-spinon contribution to $S^{+-}(\mathbf{k}, \omega)$ is defined in terms of a tight-binding model that treats spinons as free

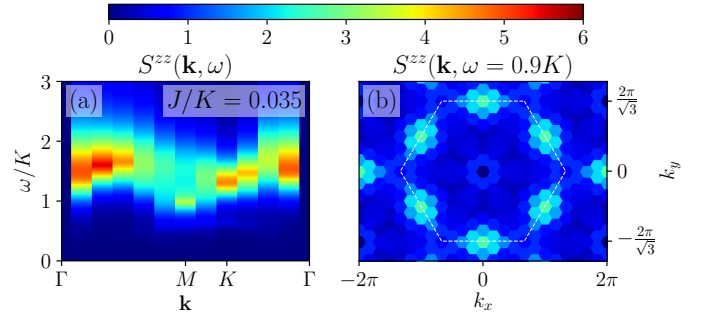


FIG. 4. DSSF $S^{zz}(\mathbf{k}, \omega)$ of the J - K model for $J/K = 0.035$, (a) along the BZ path $\Gamma \rightarrow M \rightarrow K \rightarrow \Gamma$, and (b) at $\omega = 0.9K$. The hexagon in (b) denotes the BZ.

particles¹⁹, with a dispersion relation $\epsilon_{\mathbf{k}} = \Delta_s + \epsilon_t(\mathbf{k})$, where Δ_s quantifies the local energy cost of a single spinon, and $\epsilon_t(\mathbf{k}) = -2t[\cos(\mathbf{a}_1\mathbf{k}) + \cos(\mathbf{a}_2\mathbf{k}) + \cos(\mathbf{a}_2\mathbf{k} - \mathbf{a}_1\mathbf{k})]$ the triangular lattice tight-binding dispersion with $t \sim J$ the nearest-neighbor hopping, fitted to the bandwidth of the QMC spectrum. In this approximation, $S^{+-}(\mathbf{k}, \omega) \approx \frac{4\pi}{L^2} \sum_{\mathbf{k}'} \delta(\omega - \epsilon_{\mathbf{k}'} - \epsilon_{\mathbf{k}-\mathbf{k}'})$ equals the density of two-spinon states, for which interaction effects have been accounted for phenomenologically by a Lorentzian δ -function broadening^{19,26,27}. Whereas the spectral support of $S^{+-}(\mathbf{k}, \omega)$ in Fig. 3(a) can be captured by the two-spinon model, the actual spectral weight distributions differ substantially: In particular, as already mentioned above, in the J - K model the dominant spectral weight resides along the bottom edge of the spectral support, whereas the two-spinon density of states gets suppressed in this regime and instead concentrates more towards the upper edge. While $S^{+-}(\mathbf{k}, \omega)$ in Fig. 3(a) also exhibits some spectral weight in this regime, we conclude that the spinon tight-binding model, which captures the transverse DSSF of the BFG model within the Z_2 -QSL phase rather well, is not particularly adequate for the J - K model within the anticipated QSL regime.

Upon examining the longitudinal channel, we observe more similarities in $S^{zz}(\mathbf{k}, \omega)$ between the J - K model and the BFG model QSL, than in the transverse channel: In Fig. 4(a), for $J/K = 0.035$, the excitation gap in the longitudinal channel, $\Delta_L \approx K$, is controlled by the ring exchange energy scale, which is an explicit term in the bare J - K model Hamiltonian. In fact, for the Z_2 -QSL phase of the BFG model, the gap in $S^{zz}(\mathbf{k}, \omega)$ is also of the order of the strength of the (emerging) ring exchange processes^{18,19}. However, due to the explicit presence of the ring exchange term in the J - K model, the longitudinal gap Δ_L is in this case larger than Δ_T , whereas this relation is inverted for the BFG model, for which instead Δ_L defines the lowest excitation gap.

The spectral weight distribution in Fig. 4(a) is overall remarkably similar to the BFG model result (cf. Ref. 19): In particular, we identify a dip in $S^{zz}(\mathbf{k}, \omega)$ at the M point of the BZ, which is seen more explicitly in the constant energy cut in Fig. 4(b) at $\omega = 0.9K$. For the BFG

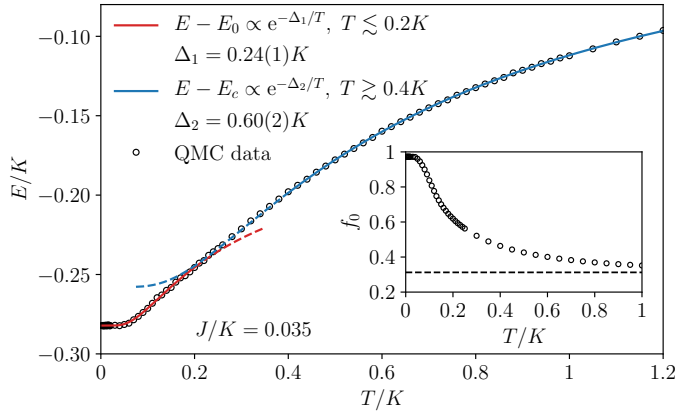


FIG. 5. Temperature dependence of the internal energy E of the J - K model for $J/K = 0.035$, along with exponential fits to activated behavior atop the ground state energy E_0 (red line) and the crossover energy $E_c \approx -0.258K$ (blue line). The inset shows the temperature dependence of the mean fraction f_0 of hexagons that satisfy the QD model subspace constraint on the longitudinal magnetization. The dashed line indicates the asymptotic value of 0.3125.

model, this repeating structure at the M points was anticipated in Refs. 18 and 19 to provide a fingerprint for crystal momentum fractionalization^{28–30} of the vison excitations within the Z_2 -QSL state, with the corresponding value of Δ_L providing the two-vison excitation gap. A similar interpretation in the present case would locate the vison excitations out of the low-energy regime (as $\Delta_L > \Delta_T$).

This hierarchy of energy scales is also imprinted in the temperature dependence of the internal energy E , shown in Fig. 5 for $J/K = 0.035$. In contrast to the BFG model^{14,18,19}, we do not observe an extended paramagnetic plateau in the temperature dependence of E in Fig. 5, cf. the less pronounced difference in the two excitation gaps Δ_L , and Δ_T in this case. Nevertheless, we can discern the observed temperature dependence in terms of two sectors: A low- T activated behavior atop the ground state energy due to the thermal proliferation of excitations with a gap of order Δ_T , and a higher- T contribution beyond a crossover energy E_c , with a larger gap of the order of Δ_L , cf. the fits in Fig. 5.

In the inset of Fig. 5, we finally examine the temperature dependence of the mean fraction f_0 of hexagons on the kagome lattice, for which the constraint $S_\odot^z = 0$ on the longitudinal magnetization (\odot denotes one of the six-site hexagons, and $S_\odot^z = \sum_{j \in \odot} S_j^z$) – defining the QD model subspace in the BFG model – is satisfied. For large temperatures, f_0 approaches the unconstrained value of $\binom{6}{3}/2^6 = 0.3125$. The fraction f_0 increases steadily upon lowering T , and in the low-temperature regime, well below the gap scales, it saturates to about 97%. The residual fluctuations from the QD model subspace are due to spin exchange processes mediated by the two-site (J) exchange terms. The J - K model thus dynamically generates the QD model subspace constraint effectively, even though an explicit penalty term, such as $\sum_\odot (S_\odot^z)^2$, is absent in its Hamiltonian (here, the summation is performed over all the hexagons of the kagome lattice).

In conclusion, we examined the DSSF of the J - K model in the two distinct regions of the low- K XY-ferromagnetic, and the large- K non-magnetic regime. For the latter, we identified two distinct excitation gaps, of which the larger one relates to the energy scale of the bare ring exchange processes of the J - K model. Moreover, the overall structure in the longitudinal channel resembles the DSSF in the QSL regime of the BFG model, hence providing spectral support for the identification in Ref. 20 of a corresponding QSL state in the J - K model. However, our results for the transverse DSSF do not further strengthen this scenario, as the spectral weight distribution for the J - K model shows qualitatively distinct features from the two-spinon continuum that is characteristic for the QSL state of the BFG model. In order to perpetuate the case for a QSL phase in the J - K model, it will thus be important to provide a compelling description of the transverse DSSF in terms of fractionalized spin excitations that accounts on a quantitative level for the QMC data that we reported here. We hope that our findings will motivate further investigations in this direction.

Acknowledgements. We thank M. Lohöfer, R. G. Melko, and F. Pollmann for useful discussions. Furthermore, we acknowledge support by the Deutsche Forschungsgemeinschaft (DFG) under grant FOR 1807 and RTG 1995, and thank the IT Center at RWTH Aachen University and the JSC Jülich for access to computing time through JARA-HPC.

¹ X.-G. Wen, Phys. Rev. B **44**, 2664 (1991).

² X.-G. Wen, Int. J. Mod. Phys. B **5**, 1641 (1991).

³ L. Balents, Nature **464**, 199 (2010).

⁴ Y. Zhou, K. Kanoda, and T.-K. Ng, Rev. Mod. Phys. **89**, 025003 (2017).

⁵ L. Savary and L. Balents, Reports on Progress in Physics **80**, 016502 (2017).

⁶ A. Y. Kitaev, Proceedings of the 3rd International Conference of Quantum Communication and Measurement, Ed.

O. Hirota, A. S. Holevo, and C. M. Caves (New York, Plenum, 1997).

⁷ A. Y. Kitaev, Ann. Phys. **321**, 2 (2006).

⁸ L. Balents, M. P. A. Fisher, and S. M. Girvin, Phys. Rev. B **65**, 224412 (2002).

⁹ D. S. Rokhsar and S. A. Kivelson, Phys. Rev. Lett. **61**, 2376 (1988).

¹⁰ P. W. Anderson, Materials Research Bulletin. **8**, 153 (1973).

- ¹¹ P. W. Anderson, *Science* **235** 1196 (1987).
- ¹² D. N. Sheng and L. Balents, *Phys. Rev. Lett.* **94**, 146805 (2005).
- ¹³ S. V. Isakov, Y. B. Kim, and A. Paramekanti, *Phys. Rev. Lett.* **97**, 207204 (2006).
- ¹⁴ S. V. Isakov, A. Paramekanti, and Y. B. Kim, *Phys. Rev. B* **76**, 224431 (2007).
- ¹⁵ S. V. Isakov, M. B. Hastings, and R. G. Melko, *Nat. Phys.* **7**, 772 (2011).
- ¹⁶ S. V. Isakov, R. G. Melko, and M. B. Hastings, *Science* **335**, 193 (2012).
- ¹⁷ Y.-C. Wang, C. Fang, M. Cheng, Y. Qi, and Z. Y. Meng, preprint arXiv:1701.01552 (2017).
- ¹⁸ G.-Y. Sun, Y.-C. Wang, C. Fang, Y. Qi, M. Cheng, and Z. Y. Meng, *Phys. Rev. Lett.* **121**, 077201 (2018).
- ¹⁹ J. Becker and S. Wessel, *Phys. Rev. Lett.* **121**, 077202 (2018).
- ²⁰ L. Dang, S. Inglis, and R. G. Melko, *Phys. Rev. B* **84**, 132409 (2011).
- ²¹ A. W. Sandvik, *Phys. Rev. B* **59**, R14157 (1999).
- ²² R. G. Melko and A. Sandvik, *Phys. Rev. E* **72**, 026702 (2005).
- ²³ F. Michel and H. G. Evertz, preprint arXiv:0705.0799 (2007).
- ²⁴ F. Michel, Ph.D. Thesis, Univ. of Graz (2007).
- ²⁵ K. S. D. Beach, preprint arXiv:cond-mat/0403055 (2004).
- ²⁶ S. Kourtis and C. Castelnovo, *Phys. Rev. B* **94**, 104401 (2016).
- ²⁷ C.-J. Huang, Y. Deng, Y. Wan, and Z. Y. Meng, *Phys. Rev. Lett.* **120**, 167202 (2018).
- ²⁸ X.-G. Wen, *Phys. Rev. B* **65**, 165113 (2002).
- ²⁹ M. Cheng, M. Zaletel, M. Barkeshli, A. Vishwanath, and P. Bonderson, *Phys. Rev. X* **6**, 041068 (2016).
- ³⁰ A. M. Essin and M. Hermele, *Phys. Rev. B* **90**, 121102(R) (2014).